Proceedings of CHT-15
ICHMT International Symposium on Advances in Computational Heat Transfer

May 25-29, 2015, Rutgers University, Piscataway, USA

CHT-15-064

A MONTE CARLO ALGORITHM BASED ON THE HYBRID TRANSPORT-DIFFUSION MODEL FOR TRANSIENT RADIATIVE TRANSFER CALCULATIONS

Maxime Roger*,§, Nicolas Crouseilles** and Pedro J. Coelho***
*Université de Lyon, INSA de Lyon, CETHIL UMR5008, F-69621 Villeurbanne Cedex, France
** INRIA-Rennes Bretagne-Atlantique (IPSO Project), Université de Rennes 1 (IRMAR), Campus de Beaulieu, 35042 Rennes Cedex, France
*** LAETA, IDMEC, Instituto Superior Técnico, Universidade de Lisboa, Av. Rovisco Pais 1, 1049-001 Lisboa, Portugal
§ Correspondence author. Fax: +33 4 72 43 88 11 Email: maxime.roger@insa-lyon.fr

ABSTRACT. In this work, a new Monte Carlo algorithm based on the hybrid-transport diffusion (HTD) model [1] is evaluated for solving the transient radiative transfer equation (RTE) in a three-dimensional problem related to optical tomography applications. The solution of the diffusion equation is used as a control-variate in the Monte Carlo algorithm in order to decrease the statistical uncertainties. The computational cost is compared to a classical MCM-RTE approach. The results show that the HTD model remains more efficient when the scattering optical thickness increases. However, in multidimensional problem, the MCM-HTD approach do not perform as well as formerly observed in one-dimensional problem [1]. It seems that the multi-scale HTD model is more efficient in hot media where emission plays a relevant role, than in cold media like those encountered in optical tomography applications.

INTRODUCTION

Optical tomography is today an attractive non-invasive technique of great interest for medical imaging [2]. In such applications, the propagation of a short-pulse laser into a biological tissue allows to determine the optical properties of the tissue and to detect inhomogeneities and tumors [3]. Short-pulse laser applications have then increased the research interest in transient radiative transfer. Accordingly various numerical methods, such as the discrete ordinate method [4, 5], the finite volume method [6] and the Monte Carlo method (MCM) [7], have been developed to solve the transient radiative transfer equation (RTE).

The statistical Monte Carlo method (MCM) is widely used in radiative transfer [8]. It is usually considered as a numerical tool for simulation of stochastic phenomena by following the statistical physics of photon transport. The MCM can also be considered as a numerical method for solving integrals. This approach links an integral formulation to a MC algorithm, and makes it possible to benefit from all available Monte Carlo optimization technique for variance reductions [9]. In transient radiative transfer, forward [7, 10, 11] and reverse algorithms [12, 13] have been developed. In a forward MCM, the optical path is randomly generated from the radiation source until its absorption, and/or its exit of the considered system, while in a reverse MCM,

based on the reciprocity principle, the bundles are tracked in a time-reversal manner from the detector to the source. The choice of using a forward or a reverse (or backward) MCM is guided by the size of the source and the detector. In transient processes, Lu and Hsu[13] pointed that one advantage of the reverse MCM is the ability to provide solutions at a given instant and at a given position, while a forward MCM requires the simulation in the whole domain, from the initial to the final time of interest.

In optically thick media, the MCM converges slowly, *i.e.*, the computational requirements increase significantly. Therefore, in this case, the macrosocopic diffusion equation (DE) can be used for modelling radiative transfer [14], despite of its drawbacks in the proximities of sources or boundaries. The DE remains very approximative but it is easier to solve, compared with the RTE, and remains consequently an attractive solution in strongly scattering media. In order to benefit from the mesoscopic RTE model and from the macroscopic DE model wherever it is appropriate, various multi-scale methods have been developed in order to improve transient radiative transfer simulations. Those multi-scale approaches are based either on decomposition methods where the RTE and the DE are coupled [15, 16, 17], or on the development of new multi-scale models such as the HTD or the micro-macro models [1, 18]. In those multi-scale models, the RTE is decomposed into a mesoscopic and a macroscopic components yielding a system of two equations, *i.e*, a macroscopic and a mesoscopic equations must be solved. In the HTD model, the macroscopic component is solution of the diffusion equation, while a transport equation, very similar to the RTE, is developed for the mesoscopic component. This transport equation allows to correct the estimation of the diffusion equation, and to obtain the solution of the RTE. It is shown in [1] that this model can be very efficient when the physical configuration is close to the diffusive regime. The aim of this work is to evaluate the HTD model proposed in [1] in the frame of the Monte Carlo method in a multidimensional test case related to optical tomography applications.

RADIATIVE TRANSFER MODELS

Radiative Transfer Equation (RTE)

The transient RTE in absorbing, emitting and scattering media can be written as

$$\frac{1}{c}\frac{\partial I}{\partial t} + \boldsymbol{u}\cdot\boldsymbol{\nabla} I = -(k_a + k_s)I + k_a I_b + k_s \int_{4\pi} p(\boldsymbol{u}|\boldsymbol{u'})I' d\boldsymbol{u'} \tag{1}$$

where $I = I(\boldsymbol{x}, \boldsymbol{u}, t)$ is the radiative intensity at location $\boldsymbol{x}$, propagation direction $\boldsymbol{u}$ and time t. $k_a(\boldsymbol{x}, t)$ is the absorption coefficient, $k_s(\boldsymbol{x}, t)$ the scattering coefficient, $p(\boldsymbol{x}, \boldsymbol{u}|\boldsymbol{u'})$ is the normalized scattering phase function and $\boldsymbol{u'}$ is the incident direction. Finally $I_b(\boldsymbol{x}, t)$ denotes the Planck function and the notation I' stands for $I' \equiv I(\boldsymbol{x}, \boldsymbol{u'}, t)$.

Problems involving collimated irradiation are usually dealt with by decomposing the radiative intensity into its collimated component I_c and its diffuse component I_d according to $I = I_c + I_d$ [19]. The collimated intensity I_c obeys the following equation :

$$\frac{1}{c}\frac{\partial I_c}{\partial t} + \boldsymbol{u}\cdot\boldsymbol{\nabla} I_c = -(k_a + k_s)I_c, \tag{2}$$

and the following transport equation is deduced for the diffuse intensity I_d:

$$\frac{1}{c}\frac{\partial I_d}{\partial t} + \boldsymbol{u}\cdot\boldsymbol{\nabla} I_d = -(k_a+k_s)I_d + k_a I_b + k_s\int_{4\pi} p(\boldsymbol{u}\cdot\boldsymbol{u'})I'_d d\boldsymbol{u'} + k_s p(\boldsymbol{u}\cdot\boldsymbol{u_c})I_c(\boldsymbol{x},\boldsymbol{u_c}) \tag{3}$$

Diffusion Equation (DE)

If the P1 approximation is assumed for the diffusive contribution $I_d \simeq \frac{1}{4\pi}G_d + \frac{3}{4\pi}\boldsymbol{j_d}\cdot\boldsymbol{u}$ as well as the diffusion approximation $\frac{\partial \boldsymbol{j_d}}{\partial t} = 0$, the DE is obtained for the calculation of $G_d = \langle I_d\rangle$ where the symbol $\langle\cdot\rangle$ represents the integral over the solid-angle space ($\langle\alpha\rangle = \int_{4\pi}\alpha(\boldsymbol{u})d\boldsymbol{u}$) :

$$\frac{1}{c}\frac{\partial G_d}{\partial t} - \boldsymbol{\nabla}\cdot(D\boldsymbol{\nabla}G_d) = k_a(4\pi I_b - G_d) + k_s I_c(\boldsymbol{x},\boldsymbol{u_c}) - \boldsymbol{\nabla}\cdot\left[3Dk_s g I_c(\boldsymbol{x},\boldsymbol{u_c})\boldsymbol{u_c}\right] \tag{4}$$

where $D = \Big(3(k_a + k_s(1-g))\Big)^{-1}$ is the diffusion coefficient and g is the anisotropic factor. The relationship between the radiative heat flux $\boldsymbol{j_d} = \langle I_d\boldsymbol{u}\rangle$ and the incident radiation G_d is given by:

$$\begin{aligned}\boldsymbol{j_d} &= -D\boldsymbol{\nabla}G_d + \frac{k_s g}{k_a + k_s(1-g)}\boldsymbol{j_c} \\ &= -D\boldsymbol{\nabla}G_d + 3Dk_s g\boldsymbol{j_c},\end{aligned} \tag{5}$$

where $\boldsymbol{j_c} = \langle I_c\boldsymbol{u}\rangle$.

Hybrid-transport diffusion model (HTD)

Using the following decomposition for the radiative intensity [1]

$$I(\boldsymbol{x},\boldsymbol{u},t) = I_c(\boldsymbol{x},\boldsymbol{u},t) + \frac{G_d(\boldsymbol{x},t)}{4\pi} + \epsilon_d(\boldsymbol{x},\boldsymbol{u},t), \tag{6}$$

and where G_d is solution of the DE (Eq. 4), the transport equation for ϵ_d is deduced from Eqs. 3 and 4:

$$\frac{1}{c}\frac{\partial \epsilon_d}{\partial t} + \boldsymbol{u}\cdot\boldsymbol{\nabla}\epsilon_d = -(k_a+k_s)\epsilon_d + k_s\int_{4\pi} p(\boldsymbol{u}\cdot\boldsymbol{u'})\epsilon'_d d\boldsymbol{u'} + S_{I_c,G_d}. \tag{7}$$

The source term S_{I_c,G_d} is written as:

$$S_{I_c,G_d}(\boldsymbol{x},\boldsymbol{u},t) = k_s I_c(\boldsymbol{x},\boldsymbol{u_c},t)\Big(p(\boldsymbol{u}\cdot\boldsymbol{u_c}) - \frac{1}{4\pi}\Big) + \frac{1}{4\pi}\Big\{\boldsymbol{\nabla}\cdot\boldsymbol{j_d} - \boldsymbol{u}\cdot\boldsymbol{\nabla}G_d\Big\} \tag{8}$$

where $\boldsymbol{j_d}$ is given by Eq. 5. The system of Eqs. 2, 4 and 7 represents the HTD model in transient radiative transfer subjected to collimated irradiation. This system of equations is strictly equivalent to the RTE.

Boundary conditions for ϵ_d

The boundary conditions for ϵ_d in the HTD model are deduced from the decomposition proposed for the radiative intensity in Eq. 6 :

$$\epsilon_d(\boldsymbol{x_w},\boldsymbol{u},t) = I_d(\boldsymbol{x_w},\boldsymbol{u},t) - \frac{G_d(\boldsymbol{x_w},t)}{4\pi} \tag{9}$$

TEST CASE

A three-dimensional cubic enclosure of side $L = 1m$ contains a scattering and absorbing homogeneous medium. The medium is subjected to a short-pulse laser beam normal to the boundary $x = 0$ of radius R as shown in figure 1. The remaining boundaries and the medium are cold (non-emitting). The phase function is isotropic. The collimated intensity, denoted by $I_{c\mathcal{L}}$,

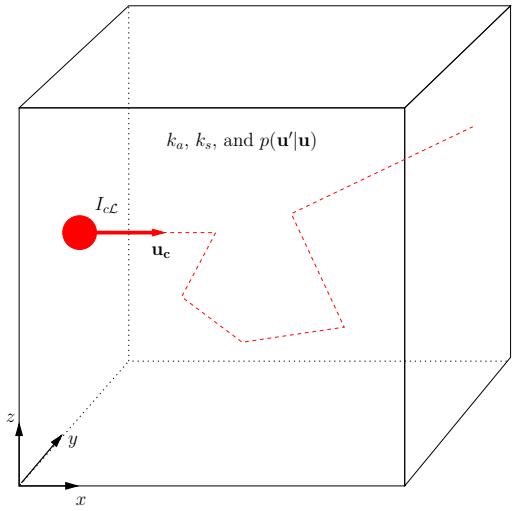

Figure 1: Test case

emitted by the short-pulse laser is Gaussian in time and uniform in space, according to :

$$I_{c\mathcal{L}}(\mathbf{r_w}, \boldsymbol{u}, t) = I_0 \delta(\boldsymbol{u} - \boldsymbol{u_c}) H(\boldsymbol{r_w} \in \mathcal{L}) \exp\Big[-4 \ln 2 \big(\frac{t - 3t_p}{t_p}\big)^2 \Big], \; 0 < t < 6t_p \tag{10}$$

where I_0 is the intensity of the laser assumed equal to unity, $\boldsymbol{u_c} = (1\ 0\ 0)$ is the collimated direction chosen normal to the boundary $x = 0$, $\boldsymbol{r_w}$ is the position defined by $(x_w = 0\ y_w\ z_w)$ and $H(\boldsymbol{r_w} \in \mathcal{L})$ is the Heaviside function equal to 1 if $\mathbf{r_w}$ is located inside the surface laser beam $\mathcal{L}$, and to 0 elsewhere. After $t = 6t_p$ where t_p is the time pulse width, the medium is free from irradiation.

MONTE CARLO ALGORITHM FOR THE RTE

Principle of integral estimation with the MCM

An integral $I = \int_{\mathcal{D}} f(\boldsymbol{x}) d\boldsymbol{x}$ over a multiple dimension domain $\mathcal{D}$ can be written by introducing an arbitrary probability density function $p_{\boldsymbol{X}}(\boldsymbol{x})$ over $\mathcal{D}$ such as :

$$I = \int_{\mathcal{D}} p_{\boldsymbol{X}}(\boldsymbol{x}) \frac{f(\boldsymbol{x})}{p_{\boldsymbol{X}}(x)} d\boldsymbol{x} = \int_{\mathcal{D}} p_{\boldsymbol{X}}(\boldsymbol{x}) w(\boldsymbol{x}) d\boldsymbol{x} \tag{11}$$

According to this formulation, the integral I is the expectation $E(W)$ of the random variable $W = \frac{f(\boldsymbol{X})}{p_{\boldsymbol{X}}(\boldsymbol{X})}$, where $\boldsymbol{X}$ is a multidimensional random variable distributed according to $p_{\boldsymbol{X}}(\boldsymbol{X})$. The function $w(\boldsymbol{x})$ is called the MC weight. In the MCM, a large number N of realizations $\boldsymbol{x}_1, \ldots, \boldsymbol{x}_N$ of $\boldsymbol{X}$ are randomly generated according to $p_{\boldsymbol{X}}$, and the corresponding MC weight

$w_i = w(\boldsymbol{x}_i) = \frac{f(\boldsymbol{x}_i)}{p_{\boldsymbol{X}}(\boldsymbol{x}_i)}$ is computed. I is estimated by the corresponding averaged value [20] :

$$I \simeq \frac{1}{N}\sum_{i=1}^{N} w_i \tag{12}$$

and a statistical uncertainty evaluated by the standard deviation of the estimator can also be computed :

$$\sigma_I \simeq \frac{1}{\sqrt{N-1}}\sqrt{\frac{1}{N}\sum_{i=1}^{N} w_i^2 - \Big(\frac{1}{N}\sum_{i=1}^{N} w_i\Big)^2} \tag{13}$$

Once presented this way, a Monte Carlo algorithm can be associated to an integral formulation and a set of probability density functions $p_{\boldsymbol{X}}$. In the remainder, the Monte Carlo algorithms are presented relying on integral formulations. More details on the link between integral and MC algorithm can be found in [9].

Monte Carlo algorithm based on the RTE (MCM-RTE)

A reverse Monte Carlo algorithm for transient radiative transfer has been proposed by Lu and Hsu in [12, 13] for homogeneous and heterogeneous media in a 1D slab, and is applied in this work to the 3D test case presented in the preceding section. The main idea is to generate an optical path in a reverse way, starting from the position and time where the radiation quantity is needed, until its exit of the system. At each new scattering position, the collimated radiation coming from the short-pulse laser is implemented in the MC weight corresponding to the optical path.

The radiation intensity $I(\boldsymbol{x}, \boldsymbol{u}, t)$ at position $\boldsymbol{x}$, direction $\boldsymbol{u}$ and time t can be written according to the integral form of the RTE [19] :

$$\begin{aligned} I(\boldsymbol{x}, \boldsymbol{u}, t) &= I(\boldsymbol{x}_w, \boldsymbol{u}, t_w)\exp\Big[-\int_0^{d_0}\beta dl\Big] + \int_0^{d_0} dl_1 \\ &\quad \exp\Big[-\int_0^{l_1}\beta(\boldsymbol{x_1})dl\Big]k_s(\boldsymbol{x_1})\int_{4\pi} p(\boldsymbol{u}|\boldsymbol{u_1})I(\boldsymbol{x_1}, \boldsymbol{u_1}, t_1)d\boldsymbol{u}_1 \end{aligned} \tag{14}$$

where $\beta = k_a + k_s$ is the extinction coefficient, $\boldsymbol{x}_w$ is the intersection between the boundary of the system and the half-line defined by the point $\boldsymbol{x}$ and the direction $-\boldsymbol{u}$, $d_0 = ||\boldsymbol{x} - \boldsymbol{x}_w||$, $\boldsymbol{x}_1 = \boldsymbol{x} - \boldsymbol{u} \times l_1$, $t_w = t - \frac{||\boldsymbol{x}-\boldsymbol{x}_w||}{c}$ and $t_1 = t - \frac{||\boldsymbol{x}-\boldsymbol{x}_1||}{c}$. The notations used in Eq. 14 are illustrated in figure 2. In our case, the radiation intensity $I(\boldsymbol{x}_w, \boldsymbol{u}, t_w)$ at the boundaries is not zero only if $\boldsymbol{x}_w$ is located on the laser surface and if $\boldsymbol{u} = \boldsymbol{u_c}$ where $\boldsymbol{u_c}$ is the collimated direction, and if $0 < t_w < 6t_p$.

Introducing the decomposition $I = I_c + I_d$ into Eq. 14 leads to :

$$\begin{aligned} I(\boldsymbol{x}, \boldsymbol{u}, t) &= I_c(\boldsymbol{x}, \boldsymbol{u}, t) + I_d(\boldsymbol{x_w}, \boldsymbol{u}, t_w)\exp\Big[-\int_0^{d_0}\beta(l)dl\Big] + \int_0^{d_0} dl_1 \exp\Big[-\int_0^{l_1}\beta(\boldsymbol{x_1})dl\Big]k_s(\boldsymbol{x_1})\Big\{ \\ &\quad p(\boldsymbol{u_c}|\boldsymbol{u_1})I_c(\boldsymbol{x_1}, \boldsymbol{u_c}, t_1) + \int_{4\pi} p(\boldsymbol{u}|\boldsymbol{u_1})I_d(\boldsymbol{x_1}, \boldsymbol{u_1}, t_1)d\boldsymbol{u}_1\Big\} \end{aligned} \tag{15}$$

where $\boldsymbol{x_w}$ is located at the boundary (see figure 2), t_w is the corresponding time $t_w = t - \frac{||\boldsymbol{x}-\boldsymbol{x_w}||}{c}$,

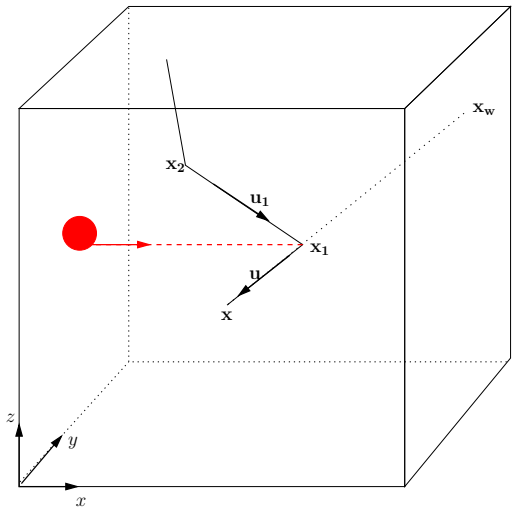

Figure 2: Illustration of the notations

and where I_c can be written as

$$I_c(\boldsymbol{x}, \boldsymbol{u}, t) = I_{c\mathcal{L}}(\boldsymbol{x_w}, \boldsymbol{u}, t_w) \exp\Big(- \int_0^{||\boldsymbol{x}-\boldsymbol{x_w}||} \beta(l) dl \Big) \tag{16}$$

where $I_{c\mathcal{L}}(\boldsymbol{x_w}, \boldsymbol{u}, t_w)$ is given by Eq. 10. In the test case, I_d is null at the boundaries of the domain : $I_d(\boldsymbol{x_w}, \boldsymbol{u}, t_w) = 0$. Therefore, the expression of the integral becomes after changing the integration domain over the length l_1 from $[0, d_0]$ to $[0, +\infty[$ and by introducing the Heaviside function H ($H(x) = 1$ if $x \geq 0$, $H(x) = 0$ if $x < 0$) :

$$\begin{aligned} I(\boldsymbol{x}, \boldsymbol{u}, t) &= I_c(\boldsymbol{x}, \boldsymbol{u}, t) + \int_0^{+\infty} dl_1 \exp\big[- \int_0^{l_1} \beta(l) dl \big] H(d_0 - l_1) k_s(\boldsymbol{x_1}) \Big\{ \\ & \quad p(\boldsymbol{u_1}|\boldsymbol{u_c}) I_c(\boldsymbol{x_1}, \boldsymbol{u_c}, t_1) + \int_{4\pi} p(\boldsymbol{u}|\boldsymbol{u_1}) I_d(\boldsymbol{x_1}, \boldsymbol{u_1}, t_1) d\boldsymbol{u_1} \Big\} \end{aligned} \tag{17}$$

The following probability density functions (pdfs) will be used in the MC algorithm :

$$p_{\boldsymbol{L}}(l) = k_s(l) \exp\Big(- \int_0^{l_1} k_s(\boldsymbol{x_1}) dl \Big) \tag{18}$$

$$p_{\boldsymbol{U_i}}(\boldsymbol{u_i}) = p(\boldsymbol{u_{i-1}}|\boldsymbol{u_i}) \tag{19}$$

$p_{\boldsymbol{L}}(l)$ can be written in the case of a homogeneous medium : $p_{\boldsymbol{L}}(l) = k_s \exp(-k_s l)$. Introducing these pdfs into the integral formulation leads to :

$$I(\boldsymbol{x}, \boldsymbol{u}, t) = \int_0^{+\infty} p_{\boldsymbol{L}}(l_1) dl_1 \int_{4\pi} p_{\boldsymbol{U_1}}(\boldsymbol{u_1}) d\boldsymbol{u_1} \int_0^{+\infty} p_{\boldsymbol{L}}(l_2) dl_2 \ldots w_{RTE} \tag{20}$$

where w_{RTE} is the Monte Carlo weight defined by :

$$\begin{aligned} w_{RTE} &= I_c(\boldsymbol{x}, \boldsymbol{u}, t) + H(d_0 - l_1) \exp\Big(- \int_0^{l_1} k_a(\boldsymbol{x_1}) dl \Big) \Big\{ p(\boldsymbol{u_c}|\boldsymbol{u_1}) I_c(\boldsymbol{x_1}, \boldsymbol{u_c}, t_1) + \\ & \quad H(d_1 - l_2) \exp\Big(- \int_0^{l_2} k_a(\boldsymbol{x_2}) dl \Big) \Big\{ p(\boldsymbol{u_2}|\boldsymbol{u_c}) I_c(\boldsymbol{x_2}, \boldsymbol{u_c}, t_2) + \ldots \Big\} \Big\} \end{aligned} \tag{21}$$

The algorithm deduced from this integral generates an optical path in a reverse way from the position $\boldsymbol{x}$ where the intensity is needed, until the exit of the system, or until the time t_i becomes lower than $t_0 = 0$ (initial time of the short-pulse emission). At each new scattering position of the optical path, the collimated radiation coming from the laser is added using Eq. 16.

MCM-RTE algorithm

- 1. The radiative intensity I is required at position $\boldsymbol{x}$, direction $\boldsymbol{u}$ and time t. $i = 1$, a loop over the N optical paths is started.
- 2. Set $j = 0$. The MC weight is initialized to $w_i = I_c(\boldsymbol{x}, \boldsymbol{u}, t)$ and the factor W to $W = 1$.
- 3. Set $j = j+1$. The optical path continues with the random generation of a path length l_j. A new scattering position is deduced $\boldsymbol{x}_j = \boldsymbol{x}_{j-1} - \boldsymbol{u_{j-1}} l_j$.
- 4. Two scenarios are possible :
  - 4.1 The position $\boldsymbol{x}_j$ is inside the domain ($l_j < d_{j-1}$). The factor W is implemented by the absorption decay $W = W \exp(-\int_0^{l_j} k_a dl)$ and the MC weight by the collimated irradiation : $w_i = w_i + W \times p(\boldsymbol{u}_{j-1}|\boldsymbol{u}_L) I_c(\boldsymbol{x_j}, \boldsymbol{u}_L, t_j)$ where the time is implemented in a reversal manner $t_j = t_{j-1} - l_j/c$. A scattered direction $\boldsymbol{u_j}$ is randomly generated according to the phase function $p(\boldsymbol{u}_j|\boldsymbol{u}_{j-1})$. Go to step 3.
  - 4.2 The position $\boldsymbol{x}_j$ is outside ($l_j > d_{j-1}$). Go to next step
- 5. If $i < N$, $i = i + 1$, go to step 2 for a new bundle. If $i = N$, the radiation intensity $I(\boldsymbol{x}, \boldsymbol{u}, t)$ is estimated according to Eq. 12 and its statistical uncertainty σ_I according to 13.

For each time t desired, a new MC run must be done. Every radiation quantity can be deduced from the radiation intensity and the corresponding MC algorithm is easily adapted for the problem considered. For instance, if the incident radiation G at point $\boldsymbol{x}$ and time t is needed, $G(\boldsymbol{x}, t) = \int_{4\pi} I(\boldsymbol{x}, \boldsymbol{u}, t) d\boldsymbol{u}$, a uniform random generation over the sphere 4π is added at step 2 in order to estimate the new integral :

- 2. $j = 0$. The MC weight is initialized to $w_i = I_c(\boldsymbol{x}, \boldsymbol{u}, t)$. A direction $\boldsymbol{u_0}$ is randomly generated according to $p_{\boldsymbol{U_0}}(\boldsymbol{u_0}) = \frac{1}{4\pi}$. The factor W is initialized to $W = 4\pi$.

This algorithm will be used as reference and compared to the MC algorithm based on the HTD model and described hereafter.

MONTE CARLO ALGORITHM FOR THE HTD MODEL (MCM-HTD)

The MCM-HTD method proposed in this work is based on the finite difference resolution of the DE, and on the Monte Carlo resolution of the mesoscopic Eq. 7.

Finite difference resolution of the DE

The Douglas-Gunn alternating direction implicit (ADI) method is applied to solve efficiently the macroscopic diffusion equation. It is a second-order method, which is quite fast, since it needs only the inversion of tridiagonal matrices to obtain an unconditionally stable solution, while a fully implicit method would require the inversion of a sparse matrix. It consists in the following three steps.

- In the first step, only the x-direction is treated semi-implicitly according to the Crank-Nicolson scheme :

$$\begin{aligned}\frac{G^{n*}_{d_{i,j,k}} - G^{n}_{d_{i,j,k}}}{c\Delta t} &= \frac{D}{2}\frac{G^{n*}_{d_{i+1,j,k}} - 2G^{n*}_{d_{i,j,k}} + G^{n*}_{d_{i-1,j,k}}}{\Delta x^2} + \frac{D}{2}\frac{G^{n}_{d_{i+1,j,k}} - 2G^{n}_{d_{i,j,k}} + G^{n}_{d_{i-1,j,k}}}{\Delta x^2} \\ &+ D\left(\frac{G^{n}_{d_{i,j+1,k}} - 2G^{n}_{d_{i,j,k}} + G^{n}_{d_{i,j-1,k}}}{\Delta y^2} + \frac{G^{n}_{d_{i,j,k+1}} - 2G^{n}_{d_{i,j,k}} + G^{n}_{d_{i,j,k-1}}}{\Delta z^2}\right) \\ &- k_a G^{n}_{d_{i,j,k}} + k_s(1 + 3D(k_a + k_s)g)I^{n}_{c_{i,j,k}} \end{aligned} \quad (22)$$

  The system of equations obtained is a tridiagonal matrix which is easily solved in order to obtain G^{n*}_d.

- In the second step, the Crank-Nicolson scheme is applied to the y-direction according to:

$$\begin{aligned}\frac{G^{n**}_{d_{i,j,k}} - G^{n}_{d_{i,j,k}}}{c\Delta t} &= \frac{D}{2}\frac{G^{n*}_{d_{i+1,j,k}} - 2G^{n*}_{d_{i,j,k}} + G^{n*}_{d_{i-1,j,k}}}{\Delta x^2} + \frac{D}{2}\frac{G^{n}_{d_{i+1,j,k}} - 2G^{n}_{d_{i,j,k}} + G^{n}_{d_{i-1,j,k}}}{\Delta x^2} \\ &+ \frac{D}{2}\frac{G^{n**}_{d_{i,j+1,k}} - 2G^{n**}_{d_{i,j,k}} + G^{n**}_{d_{i,j-1,k}}}{\Delta y^2} + \frac{D}{2}\frac{G^{n}_{d_{i,j+1,k}} - 2G^{n}_{d_{i,j,k}} + G^{n}_{d_{i,j-1,k}}}{\Delta y^2} \\ &+ D\frac{G^{n}_{d_{i,j,k+1}} - 2G^{n}_{d_{i,j,k}} + G^{n}_{d_{i,j,k-1}}}{\Delta z^2} - k_a G^{n}_{d_{i,j,k}} + k_s(1 + 3D(k_a + k_s)g)I^{n}_{c_{i,j,k}} \end{aligned} \quad (23)$$

  Again, a tridiagonal matrix must be inverted in order to compute G^{n**}_d.

- Finally, the third step leads to time $n+1$ where the semi-implicit Crank-Nicolson scheme is applied to the z-direction and to the source term.

$$\begin{aligned}\frac{G^{n+1}_{d_{i,j,k}} - G^{n}_{d_{i,j,k}}}{c\Delta t} &= \frac{D}{2}\frac{G^{n*}_{d_{i+1,j,k}} - 2G^{n*}_{d_{i,j,k}} + G^{n*}_{d_{i-1,j,k}}}{\Delta x^2} + \frac{D}{2}\frac{G^{n}_{d_{i+1,j,k}} - 2G^{n}_{d_{i,j,k}} + G^{n}_{d_{i-1,j,k}}}{\Delta x^2} \\ &+ \frac{D}{2}\frac{G^{n**}_{d_{i,j+1,k}} - 2G^{n**}_{d_{i,j,k}} + G^{n**}_{d_{i,j-1,k}}}{\Delta y^2} + \frac{D}{2}\frac{G^{n}_{d_{i,j+1,k}} - 2G^{n}_{d_{i,j,k}} + G^{n}_{d_{i,j-1,k}}}{\Delta y^2} \\ &+ \frac{D}{2}\frac{G^{n+1}_{d_{i,j,k+1}} - 2G^{n+1}_{d_{i,j,k}} + G^{n+1}_{d_{i,j,k-1}}}{\Delta z^2} + \frac{D}{2}\frac{G^{n}_{d_{i,j,k+1}} - 2G^{n}_{d_{i,j,k}} + G^{n}_{d_{i,j,k-1}}}{\Delta z^2} \\ &- k_a\frac{G^{n}_{d_{i,j,k}} + G^{n+1}_{d_{i,j,k}}}{2} + \frac{k_s(1 + 3D(k_a + k_s)g)}{2}(I^{n}_{c_{i,j,k}} + I^{n+1}_{c_{i,j,k}}) \end{aligned} \quad (24)$$

Boundary conditions for the DE

The Marshak boundary conditions are applied in this work. They assume that the following equation holds at the boundary point $\boldsymbol{x_w}$,

$$\int_{\boldsymbol{u}\cdot\boldsymbol{n}>0} \frac{G_d(\boldsymbol{x_w}, t) + 3\boldsymbol{j_d}(\boldsymbol{x_w}, t).\boldsymbol{u}}{4\pi}(\boldsymbol{u}\cdot\boldsymbol{n})d\boldsymbol{u} = \int_{\boldsymbol{u}\cdot\boldsymbol{n}>0} I_d(\boldsymbol{x_w}, \boldsymbol{u}, t)(\boldsymbol{u}\cdot\boldsymbol{n})d\boldsymbol{u} \quad (25)$$

where $\boldsymbol{n}$ is the unit normal pointing from the boundary to the medium. In the test case considered, I_d is null at the boundaries which leads to

$$\frac{G_d(\boldsymbol{x_w}, t)}{2} + \boldsymbol{j_d}(\boldsymbol{x_w}, t)\cdot\boldsymbol{n} = 0 \quad (26)$$

where $\boldsymbol{j_d}$ is given by Eq. 5. In order to achieve second-order accuracy, the central-difference approximation is used to discretize the gradient term $\boldsymbol{\nabla} G_d$ in Eq. 5.

Monte Carlo algorithm for the mesoscopic equation of the HTD

As shown in [1], once the field of G_d is estimated by the numerical resolution of the macroscopic diffusion equation, the mesoscopic Eq. 7 is solved by a MC algorithm which is similar to the reverse MC algorithm for solving the RTE.

The mesoscopic component $\epsilon_d(\boldsymbol{x}, \boldsymbol{u}, t)$ at position $\boldsymbol{x}$, direction $\boldsymbol{u}$ and time t can be written according to

$$\begin{aligned}\epsilon_d(\boldsymbol{x}, \boldsymbol{u}, t) &= \epsilon_d(\boldsymbol{x_w}, \boldsymbol{u}, t_w) \exp\Big(- \int_0^{d_0} \beta(l) dl \Big) + \int_0^{d_0} dl_1 \exp\big[- \int_0^{l_1} \beta(\boldsymbol{x_1}) dl \big] \Big\{ \\ & S_{I_c,G_d}(\boldsymbol{x_1}, \boldsymbol{u}, t_1) + k_s(\boldsymbol{x_1}) \int_{4\pi} p(\boldsymbol{u}|\boldsymbol{u_1}) \epsilon_d(\boldsymbol{x_1}, \boldsymbol{u_1}, t_1) d\boldsymbol{u}_1 \Big\} \end{aligned} \quad (27)$$

where $S_{I_c,G_d}(\boldsymbol{x_1}, \boldsymbol{u}, t_1)$ is given by Eq. 8, $t_w = t - \frac{d_0}{c}$ and $d_0 = ||\boldsymbol{x} - \boldsymbol{x_w}||$. Like for the development of the MCM-RTE algorithm, the integration domain over the length l_1 is changed from $[0, d_0]$ to $[0, +\infty[$, which gives the following formulation :

$$\begin{aligned}\epsilon_d(\boldsymbol{x}, \boldsymbol{u}, t) &= \int_0^{+\infty} dl_1 \exp\Big(- \int_0^{l_1} \beta(l) dl \Big) \Big\{ H(l_1 - d_0) \epsilon_d(\boldsymbol{x_w}, \boldsymbol{u}, t_w) + H(d_0 - l_1) \Big\{ \\ & S_{I_c,G_d}(\boldsymbol{x_1}, \boldsymbol{u}, t_1) + k_s(\boldsymbol{x_1}) \int_{4\pi} p(\boldsymbol{u}|\boldsymbol{u_1}) \epsilon_d(\boldsymbol{x_1}, \boldsymbol{u_1}, t_1) d\boldsymbol{u}_1 \Big\} \end{aligned} \quad (28)$$

Introducing the pdfs given by Eqs. 18 and 19 leads to:

$$\epsilon_d(\boldsymbol{x}, \boldsymbol{u}, t) = \int_0^{+\infty} p_{\boldsymbol{L}}(l_1) dl_1 \int_{4\pi} p_{\boldsymbol{U_1}}(\boldsymbol{u_1}) \int_0^{+\infty} p_{\boldsymbol{L}}(l_2) dl_2 \ldots w_{HTD} \quad (29)$$

where w_{HTD} is the Monte Carlo weight defined by :

$$\begin{aligned} w_{HTD} &= H(l_1 - d_0) \epsilon_d(\boldsymbol{x_w}, \boldsymbol{u}, t_w) \exp\Big(- \int_0^{d_0} k_a(\boldsymbol{x_1}) dl \Big) + H(d_0 - l_1) \exp\Big(- \int_0^{l_1} k_a(\boldsymbol{x_1}) dl \Big) \Big\{ \\ & \frac{S_{I_c,G_d}(\boldsymbol{x_1}, \boldsymbol{u}, t_1)}{k_s(\boldsymbol{x_1})} + H(l_2 - d_1) \epsilon_d(\boldsymbol{x_w}, \boldsymbol{u}, t_w) \exp\Big(- \int_0^{d_1} k_a(\boldsymbol{x_1}) dl \Big) + \\ & H(d_1 - l_2) \exp\Big(- \int_0^{l_2} k_a(\boldsymbol{x_2}) dl \Big) \Big\{ \frac{S_{I_c,G_d}(\boldsymbol{x_2}, \boldsymbol{u_1}, t_2)}{k_s(\boldsymbol{x_2})} + \ldots \Big\} \Big\} \end{aligned} \quad (30)$$

The radiation intensity $I(\boldsymbol{x}, \boldsymbol{u}, t)$ can be written as :

$$I(\boldsymbol{x}, \boldsymbol{u}, t) = I_c(\boldsymbol{x}, \boldsymbol{u}, t) + \frac{G_d(\boldsymbol{x}, t)}{4\pi} + \int_0^{+\infty} p_{\boldsymbol{L}}(l_1) dl_1 \int_{4\pi} p_{\boldsymbol{U_1}}(\boldsymbol{u_1}) \int_0^{+\infty} p_{\boldsymbol{L}}(l_2) dl_2 \ldots w_{HTD} \quad (31)$$

As in the MCM-RTE, the algorithm generates an optical path in a reverse way from the position $\boldsymbol{x}$ where the intensity is needed, until the exit of the system, or until the time t_i becomes lower than $t_0 = 0$. At each new scattering position, the source term S_{I_c,G_d} given by Eq. 8 is added to the MC weight.

MCM-HTD algorithm

- 1. Resolution of the DE according to the ADI method in order to obtain the field of the incident diffuse radiation G_d at all grid points and discrete time.
- 2. $I(\boldsymbol{x}, \boldsymbol{u}, t)$ is required. $i = 1$, a loop over the N optical paths is started.

- 3. Set $j = 0$. The MC weight is initialized to $w_i = I_c(\boldsymbol{x}, \boldsymbol{u}, t) + \frac{G_d(\boldsymbol{x},t)}{4\pi}$ and the factor W to $W = 1$.
- 4. Set $j = j+1$. The optical path continues with the random generation of a path length l_j. A new scattering position is deduced $\boldsymbol{x_j} = \boldsymbol{x}_{j-1} - \boldsymbol{u_{j-1}} l_j$.
- 5. Two scenarios are possible :
  - 5.1 The position $\boldsymbol{x_j}$ is inside the domain ($l_j < d_{j-1}$). The factor W is implemented by the absorption decay $W = W \exp(-\int_0^{l_j} k_a dl)$ and the MC weight by the source term $S_{I_c,G_d}(\boldsymbol{x_j}, \boldsymbol{u_{j-1}}, t_j)$: $w_i = w_i + W \times \frac{S_{I_c,G_d}(\boldsymbol{x_j},\boldsymbol{u_{j-1}},t_j)}{k_s(\boldsymbol{x_j})}$ where the time is implemented in a reversal manner $t_j = t_{j-1} - \frac{l_j}{c}$. A scattered direction $\boldsymbol{u_j}$ is randomly generated according to the phase function $p(\boldsymbol{u}_j|\boldsymbol{u}_{j-1})$. Go to step 3.
  - 5.2 The position $\boldsymbol{x}_j$ is outside ($l_j > d_{j-1}$). Go to next step
- 6. If $i < N$, $i = i + 1$, go to step 2 for a new bundle. If $i = N$, the radiation intensity $I(\boldsymbol{x}, \boldsymbol{u}, t)$ is estimated according to 12 and its statistical uncertainty σ_I according to Eq. 13.

Additional CPU time required for the MCM-HTD

- In the test case considered, $I_d(\boldsymbol{x_w}, \boldsymbol{u}, t_w) = 0$ which leads to $\epsilon_d(\boldsymbol{x_w}, \boldsymbol{u}, t_w) = -\frac{G_d(\boldsymbol{x_w},t_w)}{4\pi}$ according to Eq. 9. In the MCM-RTE, since $I_d(\boldsymbol{x_w}, \boldsymbol{u}, t_w) = 0$, if the generated scattering position is outside of the domain (step 4.2 of the algorithm), it is not needed to calculate the intersection point between the optical path and the boundary of the domain. In the MCM-HTD, the intersection point is needed since $\epsilon_d(\boldsymbol{x_w}, \boldsymbol{u}, t_w) \neq 0$, which requires additional CPU time.
- For the estimation of $\epsilon_d(\boldsymbol{x_w}, \boldsymbol{u}, t_w)$ at the boundary, or for the estimation of the source term S_{I_c,G_d}, the incident diffuse radiation G_d, its gradient $\boldsymbol{\nabla} G_d$, or the divergence of the diffuse radiative heat flux $\boldsymbol{\nabla}.\boldsymbol{j_d}$ are needed in the MCM-HTD at given positions $\boldsymbol{x}$, and time t. The DE resolution gives these fields at discretized time t^n and grid nodes $\boldsymbol{x}_j$, so linear interpolations are applied in order to obtain the values at the required position and time. These interpolations also require an additional cost.

In the next section, it will be investigated whether this additional computational effort is worthwhile or not.

RESULTS AND DISCUSSION

The number of grid points for the finite difference resolution of the DE has been fixed to $N_p = 50 \times 50 \times 50$ and the stability criteria CFL for the time discretization, defined such that $\Delta t = CFL \frac{\Delta x^2}{c \times D}$, has been fixed to 1. Preliminary tests have shown that increasing N_p or decreasing the CFL does not change the accuracy on the estimation of G_d.

The radius of the short-pulsed laser beam has been fixed to $0.1m$. It is centered on the position $(x = 0, y = 0.5, z = 0.5)$. The pulse width is fixed to $t_p = \frac{0.05}{c} \simeq 1.67 \times 10^{-10} s$ which corresponds to a dimensionless time parameter $t_p^* = c\tau t_p = 0.5$ when the optical thickness is $\tau = 10$. The incident radiation G at position $(x = 0.5, y = 0.2, z = 0.5)$ has been estimated with the MCM-RTE and the MCM-HTD methods and is displayed vs time in figure 3. Note that there is no direct collimated irradiation, only optical paths with at least one scattering event can reach this position. Tests have also been done at position $(x = 0.5, y = 0.5, z = 0.5)$ which is subjected to

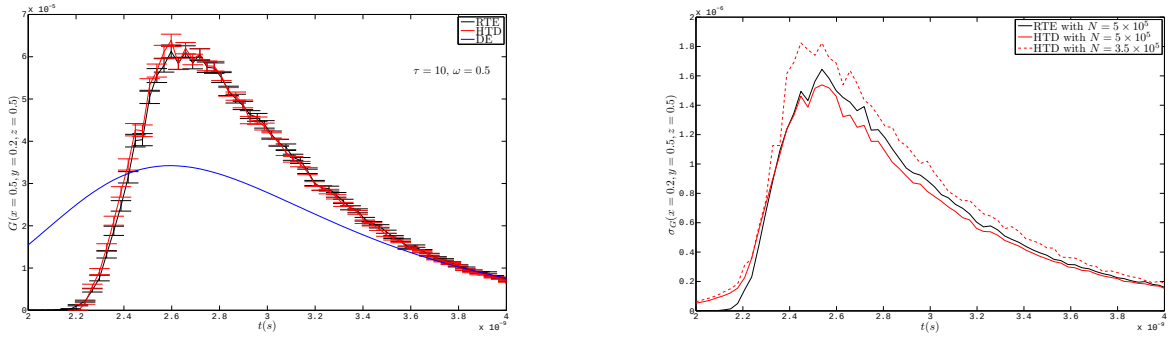

(a) (b)

Figure 3: (a) Time history of the incident radiation $G(0.5, 0.2, 0.5)$ for a number of optical paths $N = 5 \times 10^5$ estimated with the DE, MCM-RTE and MCM-HTD and (b) time history of the statistical uncertainty σ_G, for an optical thickness $\tau = 10$ and an albedo of 0.5.

direct collimated radiation. These results are not shown in this work since they are similar to the results presented hereafter (focusing on the comparison between the MCM-HTD and the MCM-RTE).

Computational cost and statistical uncertainties

As expected, it is shown in figure 3a that both methods gave the same results since the HTD model is equivalent to the RTE model. In figure 3b, the statistical uncertainties are displayed. If the same number of optical path are generated with the MCM-RTE and the MCM-HTD algorithms ($N = 5 \times 10^5$), the uncertainties on the estimations with the MCM-RTE are lower at the initial times but higher later in comparison with the MCM-HTD. At later time, the optical paths have suffered several scattering events, and therefore the diffusion approximation remains more accurate which improves the efficiency of the HTD model. However, due to the additional cost described previously, the CPU time for the MCM-HTD is higher than the CPU time for the MCM-RTE : $t_{HTD} \simeq 1.4 t_{RTE}$ (note that the time needed for the resolution of the diffusion equation is negligible $t_{RTE} \simeq 115 t_{DE}$). The statistical uncertainty for the MCM-HTD when the number of optical paths is fixed to 3.5×10^5, *i.e* , case for which the computational time is equivalent $t_{RTE}(N = 5 \times 10^5) = t_{HTD}(N = 3.5 \times 10^5)$. The statistical uncertainty for the MCM-HTD remains higher than that of the MCM-RTE. In this case, it is therefore better to use the classical MCM-RTE approach. In the remainder, the statistical uncertainties will always be compared in cases where the computational time are equivalent, *i.e.*, $t_{RTE} = t_{HTD}$.

Influence of the albedo and the optical thickness

In figure 4, the albedo is increased to 0.9. The configuration is closer to the diffusive regime, since scattering dominates now over absorption, as shown in figure 4a where the DE solution is closer to the RTE solution than in the case where $\omega = 0.5$ (in figure 3a). It can be seen again that the MCM-RTE and MCM-HTD solutions are equivalent. In figure 5b, the statistical uncertainties are displayed and it is shown that, for this case, the MCM-RTE and the MCM-HTD have an equivalent accuracy for the same computational cost.

In figure 5, the optical thickness has been increased to 20, while the albedo is still 0.9. In figure 5b, it can be seen that the MCM-HTD method becomes more efficient than the MCM-RTE.

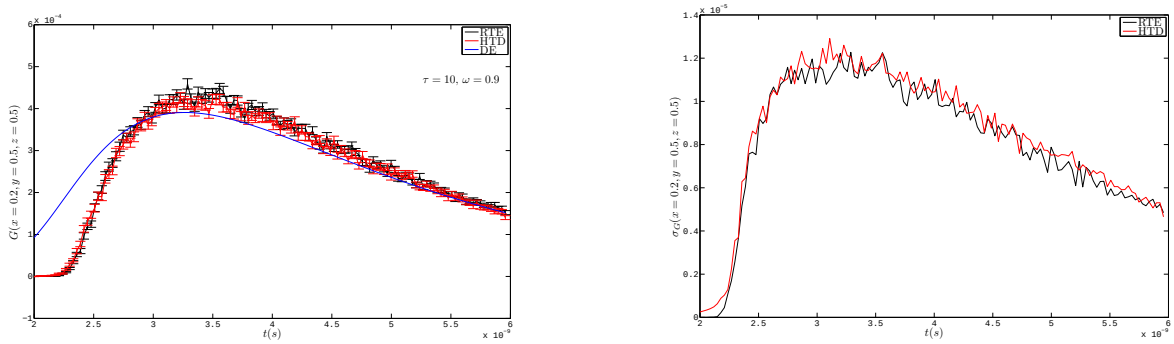

(a) (b)

Figure 4: (a) Time history of the incident radiation $G(0.5, 0.2, 0.5)$ and (b) time history of the statistical uncertainties σ_G (b), for an optical thickness $\tau = 10$, and an albedo of 0.9.

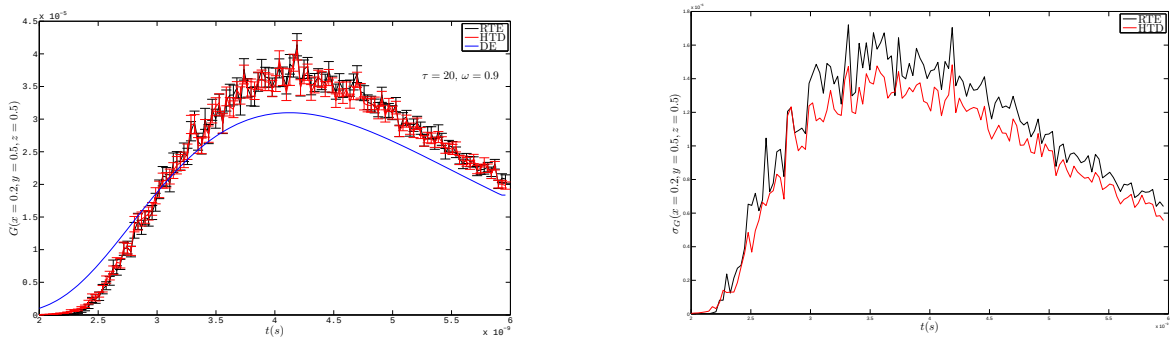

(a) (b)

Figure 5: (a) Time history of the incident radiation $G(0.5, 0.2, 0.5)$ and (b) time history of the statistical uncertainties σ_G (b), for an optical thickness $\tau = 20$, and an albedo of 0.9.

This statement confirms previous results obtained in 1D transient test case [1]. However, it may be noted that the difference between the MCM-HTD and the MCM-RTE are lower in 3D than in 1D transient test cases as those presented in [1].

CONCLUSION

The development of a Monte Carlo algorithm based on the HTD model leads to a control-variate method where the solution of the diffusion equation is used as a control variate. Indeed, the mesoscopic equation of the HTD model estimates the difference between the RTE solution and the DE solution. Therefore the MCM-HTD consist in estimating this difference instead of calculating directly the solution of the RTE like in classical MCM-RTE approach. In this work, it is shown that the MCM-HTD approach can be efficient in strongly scattering media, in medium where the radiative properties are close to various biological tissues. However, the MCM-HTD method does not ensure a better performance than the MCM-RTE in a lot of physical configurations, and do not perform as well as in one-dimensional problems. In [1], the MCM-HTD displayed efficient results in three-dimensional media in a case where the medium was not cold. Emission inside the medium increases the accuracy of the P1 approximation,

and consequently improves the efficiency of the HTD approach. In conclusion, the HTD model remains a good alternative to the RTE when the medium is close to the diffusive regime, but it is shown in this work that its efficiency remains limited in optical tomography applications where cold media are generally considered.

In future work, an interesting approach would be to use a decomposition method where the domain is split into a subdomain where the RTE is solved, and a subdomain (where the diffusion approximation gives relatively good results) where the HTD model is used, similarly to the approach proposed in [16]. Indeed, one specific advantage of the HTD model is to allow an easy treatment of the interface between the two sub-domains and therefore to offer an interesting frame for the develoment of multi-scale methods based on decomposition method. The extension to heterogeneous media of the MCM-HTD can be envisaged without additional methodological difficulties. The algorithm presented in this work is based on formulations adapted to heterogeneous media, i.e, the extension is therefore straightforward. The difficulties linked to the treatment of the heterogeneities are the same than in the MCM-RTE, and efficient approaches such as the null-collision algorithms [21] can be applied to overcome this problem.

ACKNOWLEDGMENTS

Financial support of FCT-Fundação para a Ciência e a Tecnologia within the framework of project PTDC/EMS-ENE/1028/2012 is acknowledged.

REFERENCES

[1] M. Roger, C. Caliot, N. Crouseilles, and P.J. Coelho, "A hybrid transport-diffusion model for radiative transfer in absorbing and scattering media", *J. Comput. Phys.*, vol. 275, pp. 346–362, 2014.

[2] A.J. Welch and M.J.C. van Gemert, Eds., *Optical-thermal response of laser-irradiated tissue*, Plenum, New York, 1995.

[3] S. Kumar and K. Mitra, "Microscale aspects of thermal radiation transport and laser application", *Adv Heat Transfer*, vol. 33, pp. 187–294, 1999.

[4] Z. Guo and K. Kim, "Ultrafast-laser-radiation transfer in heterogeneous tissues with the discrete-ordinate method", *Appl. Opt.*, vol. 42, pp. 2897–2905, 2003.

[5] I. Ayranci and N. Selçuk, "MOL solution of DOM for transient radiative transfer in 3-d scattering media", *J. Quant. Spectrosc. Radiat. Transf.*, vol. 84, pp. 409–422, 2004.

[6] J.C. Chai, "Finite volume method for transient radiative transfer", *Numerical Heat Transf., Part B*, vol. 44, pp. 187–208, 2003.

[7] SL. Jacques, *Optical-thermal response of laser-irradiated tissue, chapter 5 : Monte Carlo modeling of Light Transport in Tissue (Steady State and Time of Flight)*, A.J. Welch and M.J.C. van Gemert, Plenum, New York, 1995.

[8] J.R. Howell, "The Monte Carlo method in radiative heat transfer", *J. Heat Transf.*, vol. 120, no. 3, pp. 547–560, 1998.

[9] J. Delatorre and et al., "Monte Carlo advances and concentrated solar applications", *Solar Energy*, vol. 103, pp. 653–681, 2014.

[10] M.Q. Brewster and Y. Yamada, "Optical properties of thick, turbid media from picosecond time-resolved light scattering measurements", *Int. J. Heat Mass Transf.*, vol. 38, no. 14, pp. 2569–2581, 1995.

[11] Z. Guo, J. Aber, BA. Garetz, and S. Kumar, "Monte Carlo simulation and experiments of pulsed radiative transfer", *J. Quant. Spectrosc. Radiat. Transf.*, vol. 73, pp. 159–168, 2002.

[12] X. Lu and P f. Hsu, "Reverse Monte Carlo simulations for transient radiative transfer in participating media", *J. Heat Transf.*, vol. 126, no. 4, pp. 621–627, 2004.

[13] X. Lu and P f. Hsu, "Reverse Monte Carlo simulations of light pulse propagation in nonhomogeneous media", *J. Quant. Spectrosc. Radiat. Transf.*, vol. 93, pp. 349–367, 2005.

[14] Z. Guo, S.K. Wan, K. Kim, and C. Kosaraju, "Comparing diffusion approximation with radiation transfer analysis for light transport in tissues", *Optical Review*, vol. 10, no. 5, pp. 415–421, 2003.

[15] D. Gorpas, D. Yova, and K. Politopoulos, "A three-dimensional finite elements approach for the coupled radiative transfer equation and diffusion approximation modeling in fluorescence imaging", *J. Quant. Spectrosc. Radiat. Transf.*, vol. 111, pp. 553–568, 2010.

[16] M. Roger and N. Crouseilles, "A dynamic multi-scale model for transient radiative transfer calculations", *J. Quant. Spectrosc. Radiat. Transf.*, vol. 116, pp. 110–121, 2013.

[17] O. Lehtikangas and T. Tarvainen, "Hybrid forward-peaked-scattering-diffusion approximations for light propagation in turbid media with low-scattering regions", *J. Quant. Spectrosc. Radiat. Transf.*, vol. 116, pp. 132–144, 2013.

[18] M. Roger, N. Crouseilles, and P.J. Coelho, "The micro-macro model for transient radiative transfer simulations", in *Proceedings of the 15th International Heat Transfer Conference, IHTC-15*, 2014.

[19] M.F. Modest, *Radiative heat transfer*, New-York: McGraw-Hill, 2003.

[20] J.M. Hammersley and D.C. Handscomb, *Monte Carlo Methods*, Chapman and Hall, London, 1964.

[21] M. Galtier, S. Blanco, C. Caliot, C. Coustet, J. Dauchet, M. El Hafi, and et al., "Integral formulation of null-collision Monte Carlo algorithms", *J. Quant. Spectrosc. Radiat. Transf.*, vol. 125, pp. 57–68, 2013.